Biomolecular study and conjugation of two para-aminobenzoic acid derivatives with serum proteins: drug binding efficacy and protein structural analysis

P. Chanphai, F. Cloutier, Y. Oufqir, M.-F. Leclerc, A.M. Eiján, C. Reyes-Moreno, G. Bérubé & H.A. Tajmir-Riahi

Accepted author version posted online: 24 Jan 2020.

Submit your article to this journal ⬦

Article views: 11

View related articles ⬦

View Crossmark data ⬦

<u>**Short title**</u>: Conjugation of para-aminobenzoic acid derivatives with serum proteins

Biomolecular study and conjugation of two para-aminobenzoic acid derivatives with serum proteins: drug binding efficacy and protein structural analysis

P. Chanphai[1], F. Cloutier[1,3], Y. Oufqir[2,3], M.-F. Leclerc[1,3], A.M. Eiján[4], C. Reyes-Moreno[2,3], G. Bérubé[1,3*] and H.A. Tajmir-Riahi[1*]

[1]Department of Chemistry, Biochemistry and Physics, University of Quebec at Trois-Rivières, 3351, boul. des Forges, Trois-Rivières (Québec) G8Z 4M3, Canada;

[2]Department of Medical Biology, University of Québec at Trois-Rivières, 3351, boul. des Forges, Trois-Rivières (Québec) G8Z 4M3, Canada

[3]Groupe de Recherche en Signalisation Cellulaire, University of Québec at Trois-Rivières, 3351, boul. des Forges, Trois-Rivières (Québec) G8Z 4M3, Canada;

[4]Facultad de Medicina, Universidad de Buenos Aires, Av. San Martín 548, Ciudad de Buenos Aires - C1417DTB, Argentina (anamaiaeijan@gmail.com).

*Corresponding authors: E-mail: tajmriri@uqtr.ca and Gervais.Berube@uqtr.ca Fax: 819-376-5084; Tel: 819-376-5011 (ext. 3326)

Abstract

Two aminobenzoic acid derivatives DAB-0 and DAB-1 showed distinct biological properties on murine bladder cancer (BCa) cell line MB49-I. In contrast to DAB-1, DAB-0 does not possess any anti-inflammatory activity and is less toxic. Furthermore, DAB-0 does not interfere with INFγ-induced STAT1 activation and TNFα-induced IκB phosphorylation, while DAB-1 does. In order to rationalize these results, the binding efficacy of DAB-0 and DAB-1 with serum proteins such a human serum albumin (HSA), bovine serum albumin (BSA) and beta-lactoglobulin (β-LG) was investigated in aqueous solution at physiological

pH. Multiple spectroscopic methods and thermodynamic analysis were used to determine the binding efficacy of DAB-0 and DAB-1 with serum proteins. Drug-protein conjugation was observed *via* through ionic contacts. DAB-1 forms stronger adducts than DAB-0, while *β*-LG shows more affinity with the order of stability *β*-LG > BSA > HSA. The stronger complexation of DAB-1 with serum proteins might account for its biological potential and transport in the blood. The binding efficacy ranged from 40 to 60%. Major alterations of protein secondary structures were detected upon drug complexation. Serum proteins are capable of delivering DAB-1 *in vitro*.

Keywords: DAB-0, DAB-1, serum protein, delivery, binding efficacy, thermodynamic analysis

Abbreviations: BSA, bovine serum albumin; (DAB-0), *N′*-[4-(2,5-dioxo-pyrrolidin-1-yl)-benzoyl]-hydrazine carboxylic acid *tert*-butyl ester (DAB-1), *N′*-[4-(2,5-dioxo-2,5-dihydro-pyrrol-1-yl)-benzoyl]-hydrazine carboxylic acid *tert*-butyl est ;HSA. Human serum albumin; FTIR, Fourier transform infrared; *β*-LG, beta-lactoglobulin.

Introduction

Inflammation plays an important role in the initiation and progression of several types of cancers including bladder cancer, prostate cancer and breast cancer (Colotta et al., 2009; Sui et al., 2017). Hence there is a renewed scientific interest in the development of novel anti-inflammatory treatment strategies able either to circumvent cancer inflammation and/or to enhance the curative impact of known drugs (Zhu et al., 2012; Nakamura et al., 2017; Dai et al., 2017). Recently, we studied the anti-inflammatory and anticancer/antimetastatic properties of small aminobenzoic acid derivative namely, DAB-1 (Hamelin-Morrissette et al., 2015). In that paper, we reported that both portions of the molecules are necessary for its biological action. Indeed, the maleimide as well as the *tert*-butoxycarbonyl moieties of

DAB-1 are critical for its anti-inflammatory activity and its anticancer properties. Furthermore, we showed that DAB-1 (**Scheme 1**) efficiently inhibits cytokine-induced expression of pro-inflammatory genes and motility in human M1 macrophages (Hamelin-Morrissette et al., 2015). We disclosed that DAB-1 could inhibit the production of NO, a pro-tumor inflammatory mediator, in murine urothelial bladder carcinoma cells and macrophages. Because the maleimide portion is required for its anti-inflammatory properties, DAB-1 was hydrogenated (Berube & Reyes-Moreno, 2017). The hydrogenation and the loss of double bound in the maleimide moiety was confirmed by standard spectrometric analysis (Berube & Reyes-Moreno, 2017). The anti-inflammatory properties of DAB-0 was investigated by its ability to inhibit NO production in murine macrophage cells (Berube & Reyes-Moreno, 2017). However, once the maleimide portion is hydrogenated the molecule, called DAB-0, loses its anti-inflammatory properties (Berube & Reyes-Moreno, 2017). Therefore, in order to understand the possible role and implication of the maleimide portion of DAB-1, the comparison with DAB-0 needed to be investigated. In this study, to further investigate the anticancer potential of these molecules, the anti-proliferative activity, the anti-inflammatory activity and cell signaling pathways were determined in the murine bladder cancer (BCa) cell line MB49-I, a highly invasive and tumorigenic BCa cell model (Hamelin-Morrissette et al., 2015). As well, the interactions of these molecules with serum proteins were investigated to provide additional insight into its mode of transport in the blood.

Serum proteins contain multiple binding sites with different affinities and can transport diverse drugs, fatty acids, steroid hormones and many other bioactive materials (Yang et al., 2014; Ghuman et al., 2005; Kratochwil et al., 2002; Ahmed-Ouameur et al., 2006). Serum

albumins are emerging as versatile protein carriers for drug targeting systems and for improving the pharmacokinetic profile of peptides or protein-based drugs (Elsadek & Kratz, 2012; Kratz & Elsadek, 2012; Kratz, 2008). In order to evaluate the potential application of serum proteins in delivery of DAB-1, it was of interest to compare the binding efficacy of this drug to serum proteins in aqueous solution. The reference inactive analog DAB-0 was also assessed to contrast the results obtained with DAB-1. Recent studies showed encapsulation of testosterone and its dimeric derivatives by serum proteins (Chanphai et al., 2015a; Chanphai et al., 2015b). Carrier proteins such as HSA, BSA and β-LG, show different hydrophobicity (Akdogan et al., 2012; Jamson et al., 2012); Chanphai et al., 2018) and exhibit different affinity towards drug interactions.

The biological activity and conjugation of DAB-0 and DAB-1 (**Scheme 1**) with human and bovine serum albumins and β-lactoglobulin was investigated, using multiple spectroscopic methods and thermodynamic analysis. Furthermore, the possibility of delivery of DAB-0 and DAB-1 by serum proteins is discussed herein.

DAB-0   **DAB-1**
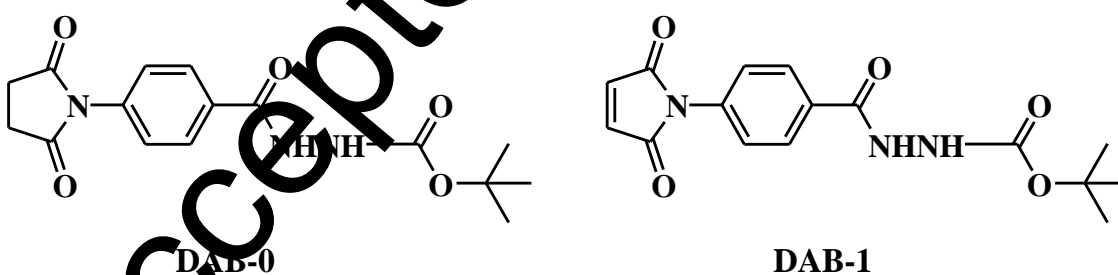
Scheme 1: Chemical structures of DAB-0 and DAB-1

Experimental

Biological evaluation

Cell culture

Biological assays were performed using the murine bladder cancer (BCa) cell line MB49-I, as we previously described (Hamelin-Morrissette et al., 2015). The cell line MB49-I is a highly invasive and tumorigenic BCa cell model that was developed by successive *in vivo* passages of MB49 primary tumors (Fabris et al., 2012). The cells were maintained in RPMI medium supplemented with 10% heat-inactivated fetal bovine serum (FBS) and containing 1 mM sodium pyruvate, 10 mM 4-(2-hydroxyethyl)-piperazine-1-ethanesulfonic acid (HEPES) and 50 μg/mL gentamycin (referred as 10% FBS RPMI-1640). The cells were maintained at 37 ºC in a moisture-saturated atmosphere containing 5% CO_2.

Evaluation of cell proliferation by the MTT assay

To evaluate and compare the anti-proliferative activity between DAB-0 and DAB-1, cell viability/proliferation MTT assays were performed as previously described (Carmicheal et al., 1987; Dallagi et al., 2015; Dufresne et al., 2011; Dumas et al., 2013; Leduc et al., 2012). Briefly, MB49-I cells (5×10^3 cells/well) were plated in 96-well plates in 100 μL 10% FBS RPMI-1640 and cultured for 24 h at 37°C and 5% CO_2. Cells were pretreated for a period of 30 min with vehicle (DMSO) or compounds DAB-0 and DAB-1 at different increasing concentrations (15, 30, 60 and 90 μM), and then activated for 24 h with 5 ng/mL IFNγ and 25 ng/mL TNFα. At the end of the culture period, the culture media for each experimental point was transferred into new 96-well plates to assess NO production (see next sub-section), and the well containing the cells were replenished with 100 μL phosphate-buffered solution (PBS) to assess MTT assays. For this purpose, 10 μL of 5 mg/mL methylthiazolyldiphenyl-tetrazolium bromide (MTT) solution was added to each well containing 100 μL PBS. After a 3-h incubation period with MTT reagent, 100

μL of MTT solubilization buffer (10% SDS in 10 mM HCl) was added and plates were placed overnight in the cell incubator before absorbance measure. The optical density was read at 580 nm using the Microplate Reader Manager (from Bio-Rad Laboratories).

Evaluation of NO production by the Griess reagent method

NO production was measured using the Griess reagent method as previously described [26]. This method involves the detection of nitrite ions (NO_2^-) formed by the spontaneous oxidation of NO under physiological conditions. According to the manufacturer protocol (Life Technologies; # G-7921), equal volumes of sulfanilic acid and N-(1-naphthyl) ethylenediamine are mixed together to form the Griess reagent. In contact with NO_2^-, present in the supernatant from the above pretreated and activated MB49-I cells, the sulfanilic acid is converted to a diazonium salt, which in turn is coupled to N-(1-naphthyl) ethylenediamine to produce a pink coloration that is measured with a spectrophotometer (Biotek, synergy HT) at 548 nm.

Cell signaling studies

MB49-I cells (25×10^4 cells/well) were pretreated for 30 min with vehicle (DMSO) or compounds DAB-0 and DAB-1 at different increasing concentrations (15, 30 and 60 μM), and then washed and recovered after 15 min of activation with 5 ng/mL IFNγ or after 5 min of activation with 25 ng/mL TNFα. Cell lysates were prepared and analyzed by immunoblotting as described (Dallagi et al., 2015; Dufresne et al., 2011; Dumas et al., 2013; Leduc et al., 2012). Briefly, protein samples were resolved by SDS-PAGE under reducing conditions and transferred onto a PVDF membrane. Blots were first probed with

rabbit polyclonal antibodies against phospho-STAT1 (pSTAT1) and p-IκB (both at 1:2000) overnight at 4°C. Blots were then incubated with HRP-conjugated goat anti-rabbit IgG Ab (1:3000) for 1 h at room temperature. The same blots were stripped and then probed with anti-STAT1 (at 1:1000) and anti-β-actine (1:4000) antibodies. In both cases, probed molecules were visualized using an enhancement chemiluminescence detection kit (Thermo Fisher Scientific).

Chemistry

Materials

HSA, BSA fraction V and *β*-lactoglobulin (A variant, purity >90) were purchased from Sigma Chemical Company (St-Louis, MO) and used as supplied. DAB-0 and DAB-1 were synthesized in our laboratory using a three-step (DAB-1) or four-step (DAB-0) reaction sequence from *para*-aminobenzoic acid as reported earlier (Leduc et al., 2012; Belgorosky et al., 2014). The compounds were fully characterized by IR, ^{1}H-NMR, ^{13}C-NMR spectroscopy and by mass spectrometry. Other chemicals were of reagent grade and used without further purification.

Preparation of DAB-0 and DAB-1-protein complexes

Appropriate amounts of protein (BSA, HSA or *β*-LG) were dissolved in aqueous solution (125 μM) containing 10 mM Tris-HCl (pH 7.2). BSA and HSA concentrations were determined spectrophotometrically using the extinction coefficient of 36500 M^{-1} cm^{-1} at 280 nm (Painter et al., 1998). *β*-LG concentration was determined spectrophotometrically using the extinction coefficient of 17600 M^{-1} cm^{-1} at 280 nm (Collini et al., 2000). DAB-0 and DAB-1 (200 μM) were dissolved in water-ethanol (50/50%) and then diluted by serial dilution to different concentrations in Tris-HCl (pH 7.2).

UV spectroscopy

The UV-Vis spectra were recorded on a Cary 60 UV-Visible spectrophotometer with a slit of 2 nm and scan speed of 400 nm min^{-1}. Quartz cuvettes of 1 cm were used. The absorbance measurements were performed at pH 7.2 by keeping the concentration of protein constant (60 µM), while increasing drug concentrations (1 µM to 60 µM). The binding constants of drug-protein complexes were determined as reported (Zhong et al., 2004).

FTIR spectroscopy

Infrared spectra were recorded on a FTIR spectrometer (Impact 420 model), equipped with deuterated triglycine sulphate (DTGS) detector and KBr beam splitter, using AgBr windows. Solution of DAB drug was added dropwise to the protein solution with constant stirring to ensure the formation of a homogeneous solution and to reach the target drug concentrations of 15, 30 and 60 µM with a final protein concentration of 60 µM. Interferograms were accumulated over the spectral range 4000–600 cm^{-1} with a nominal resolution of 2 cm^{-1} and 100 scans. The difference spectra [(protein solution + drug solution) − (protein solution)] were generated using water combination mode around 2300 cm^{-1}, as standard (Dousseau et al., 1989). When producing difference spectra, this band was adjusted to the baseline level, in order to normalize difference spectra. Analysis of the secondary structures of protein and the drug complexes were carried out as reported (Byler & Susi, 1986; Beauchemin et al., 2007). The curve-fitting analysis was performed using the GRAMS/AI Version 7.01 software of the Galactic Industries Corporation.

Molecular modeling

The structure of free HSA (PDB id:1AO6, chain A) obtained by X-ray crystallography was used as a template (Sugio et al., 1999). The structure of BSA was predicted by automated homology modeling using SWISS-MODEL Workspace from the amino acid sequence NP-851335 [Arnol et al., 2006; Rost, 1999; Bourassa et al., 2011). The two proteins share 78.1% of sequence identity, which is sufficient to obtain reliable sequence alignment. The βLG structure was obtained from the literature report (Loch et al., 2015). The docking studies were performed with ArgusLab 4.0.1 software (Mark A. Thompson, Planaria Software LLC, Seattle,WA, http://www.arguslab.com). Three-dimensional structures of DAB-0 and DAB-1 were generated from PM3 semi-empirical calculations, using Chem3D Ultra 6.0.

Statistical analyses

For all biological assays, data were presented as mean ± SEM from three independent experiments. Data were analyzed by one-way ANOVA followed by Bonferonni post-test using Prism software, version 3.03 (GraphPad, San Diego, CA). p values of ≤ 0.05 were considered to indicate statistical significance.

Results and discussion

Anti-proliferative activity of DAB-0 and DAB-1

The anti-proliferative activity of the molecules was evaluated using the MTT assay on murine BCa cell line MT49-1 (Hamelin-Morrissette et al., 2015). The results from the anti-proliferative activity assay are shown in **Fig. 1A**. DAB-0 is essentially non-toxic up to the highest concentration used; 90 μM. However, DAB-1 displays significant cytotoxicity at concentrations of 60 and 90 μM, but remains not toxic up to a concentration of 30 μM. The anti-proliferative result clearly contrast the discrepancy between both DAB molecules; DAB-1 is more cytotoxic than DAB-0, the latter being nontoxic towards BCa cells.

Anti-inflammatory activity

The anti-inflammatory activity was evaluated by measuring NO production in murine BCa cell line MB49-I stimulated by two powerful pro-inflammatory cytokines, INFγ and TNFα, and using the Griess reaction methodology (Belgorosky et al., 2014). **Figure 1B** presents the results obtained from this study. DAB-0 did not decrease NO production by the cells at any of the concentration tested. Contrarily, DAB-1 significantly decreased NO production starting at a concentration as low as 30 μM. At 15 μM no effect was detected for both compounds. This assay confirms that DAB-1 possesses significant anti-inflammatory activity in comparison to DAB-0 that displays none.
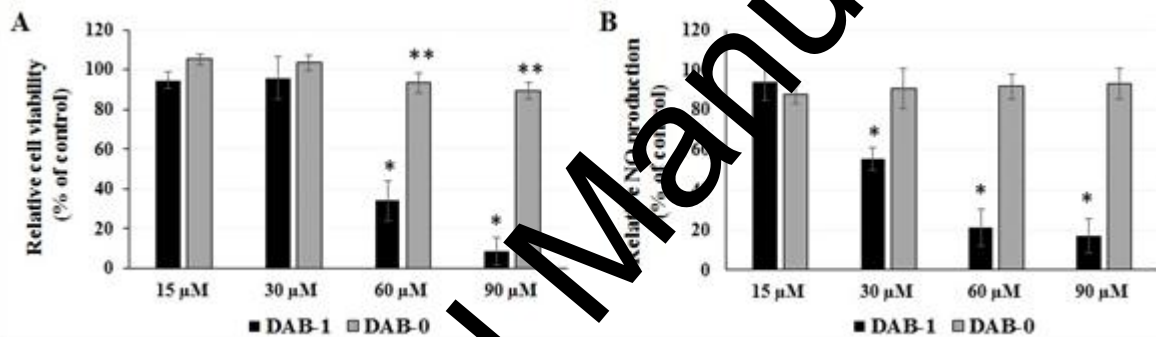
Figure 1. Graphical representation of relative cell viability (A) and NO production (B) in the murine BCa cell line MB49-I which were pretreated for 30 min with vehicle (DMSO) or the compounds DAB-1 and DAB-0 at different concentrations, and activated for 24 h with the pro-inflammatory cytokines IFNγ and TNFα. Mean ± SEM was obtained from three independent measurements. ** $p < 0.01$ denote significant difference compared to control (DMSO) for each DAB-1 or DAB-0 dose.

Cell signaling studies

To study the anti-cancer potential of DABs, we investigated the activation status of two major pro-inflammatory and pro-tumor signaling pathways in MB49-I cells; IFNγ/STAT3 and TNFα/NFκB. In order to test the first signaling pathway, cells were pretreated with DMSO (control) and activated for a period of 15 minutes with INFγ triggering STAT3

activation. Naturally, PBS stimulation did not activate STAT-1. In contrast, in response to INFγ activation, pretreatment with DAB-1 at 30 and 60 μM drastically decreases the formation of p-STAT1 in comparison to DAB-0, which displays no effect at any of the concentrations tested (**Figs 2A and 2B**).

For the second signaling pathway, the cells were activated with TNFα for 5 minutes initiating the production of p-IκB. Control cells were treated with PBS without effect on NFκB activation. As shown in figure 2C and 2D, DAB-1 inhibits NFκB activation at concentration as low as 15 μM. In comparison, DAB-0 only slightly inhibited the production of p-IκB at the highest concentration tested (60 μM).

Taken together, these results suggest that DAB-1 but not DAB-0, effectively inhibited IFNγ/STAT3 and TNFα/NFκB signaling pathways activation in MB49-I cells. Hence, DAB-1 is an anti-inflammatory molecule via the inhibition of NO production and has the ability to inhibit pro-inflammatory and pro-tumor pathways by the inhibition of STAT-1 and IκB phosphorylation/activation.
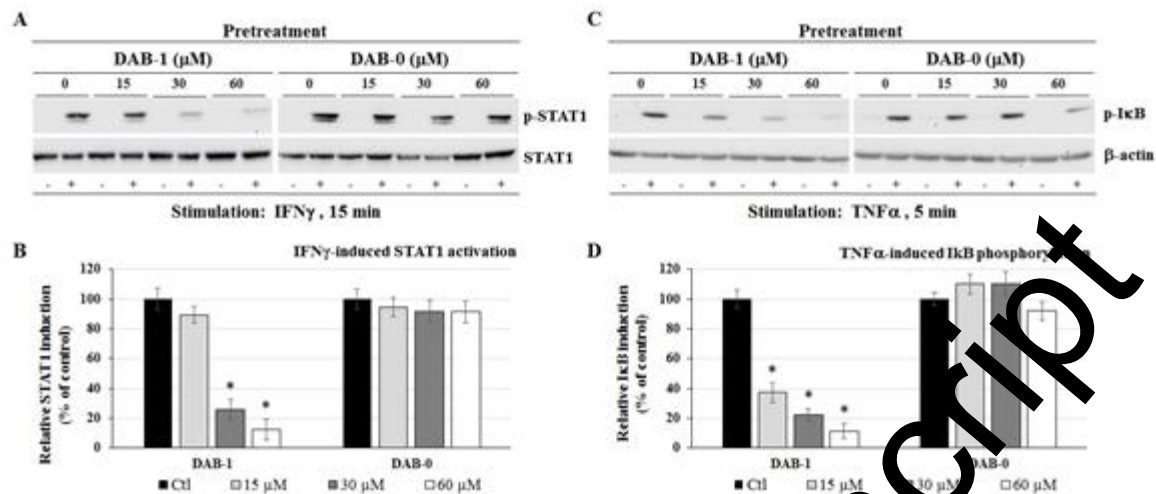
Figure 2. Representative images (A) and graphical analysis (B) of phosphorylated STAT1 (p-STAT1) in MB49-I cells pretreated for 30 min with vehicle (DMSO) or the compounds DAB-1 and DAB-0 at different concentrations, and activated for 15 minutes with PBS (-) or 5 ng/mL IFNγ (+). Representative images (C) and graphical analysis (D) of phosphorylated IκB (p-IκB) in MB49-I cells pretreated for 30 min with vehicle (DMSO) or the compounds DAB-1 and DAB-0 at different concentrations, and activated for 5 minutes with PBS (-) or 25 ng/mL TNFα (+). Mean ± SEM was obtained from three independent measurements. * $p < 0.01$ and ** $p < 0.05$ denote significant difference compared to control (DMSO) for each DAB-1 or DAB-0 dose.

Stability of DAB-0 and DAB-1-protein complexes by UV spectroscopy

The DAB-0 and DAB-1 complexation with serum proteins induces major changes in the absorption spectra of protein and this can be used to calculate the drug-protein binding constants. The UV spectra of drugs with HSA, BSA and β-LG complexes are presented in **Figs 3** and **4**. Drug conjugation with protein occurred with an increase in the intensity of protein band at 280 nm.

The drug-protein binding constants were calculated as described in materials and methods (Zhong et al., 2004), using plots of $1/(A-A_0)$ vs (1/drug concentrations) (**Figs 3** and **4**), where A_0 is the initial absorbance of the free protein at 280 nm and A is the recorded

absorbance of complexes at different drug concentrations (**Figs 3, 4** and **Table 1**). The results showed that strong drug-protein interactions were observed with the order of stability β-LG > drug-BSA > drug-HSA with DAB-1 forming stronger conjugates than DAB-0 (**Figs 3, 4** and **Table 1**). In part, this could explain the observed biological activity of DAB-1 in comparison to DAB-0, the inactive analog. Experimental evidence regarding hydrophobic, hydrophilic or H-bonding contacts comes from the thermodynamic analysis of drug-protein complexes discussed below.

Table 1. Variations of the binding constants for DAB -0 and DAB -1 with serum proteins at different temperatures

Complexes	Temperature (K)	Binding constant $K(mol/L)^{-1}$
DAB - 0 – HSA	298.15	1.18×10^5
	308.15	8.52×10^4
	318.15	6.23×10^4
DAB - 1 – HSA	298.15	1.30×10^5
	308.15	9.15×10^4
	318.15	7.38×10^4
DAB - 0 – BSA	298.15	9.32×10^4
	308.15	7.50×10^4
	318.15	5.60×10^4
DAB - 1 – BSA	298.15	9.59×10^4
	308.15	8.93×10^4
	318.15	8.42×10^4
DAB - 0 – β - LG	298.15	4.00×10^5
	308.15	3.68×10^5
	318.15	3.35×10^5
DAB - 1 – β - LG	298.15	5.95×10^5
	308.15	4.21×10^5
	318.15	3.39×10^5

Figure 3

Figure 3. UV-visible spectra of DAB-0 and its conjugates with HSA (**A**), BSA (**B**) and β-LG (C) at 60 μM (a) and its DAB-0 complexes (b-i) for DAB-1 at 1, 5, 10, 20, 30, 40, 50 and 60 μM; Inset: plot of $1/(A-A_0)$ vs $(1/$ drug concentration) and binding constants (*K*) for drug-protein conjugates.
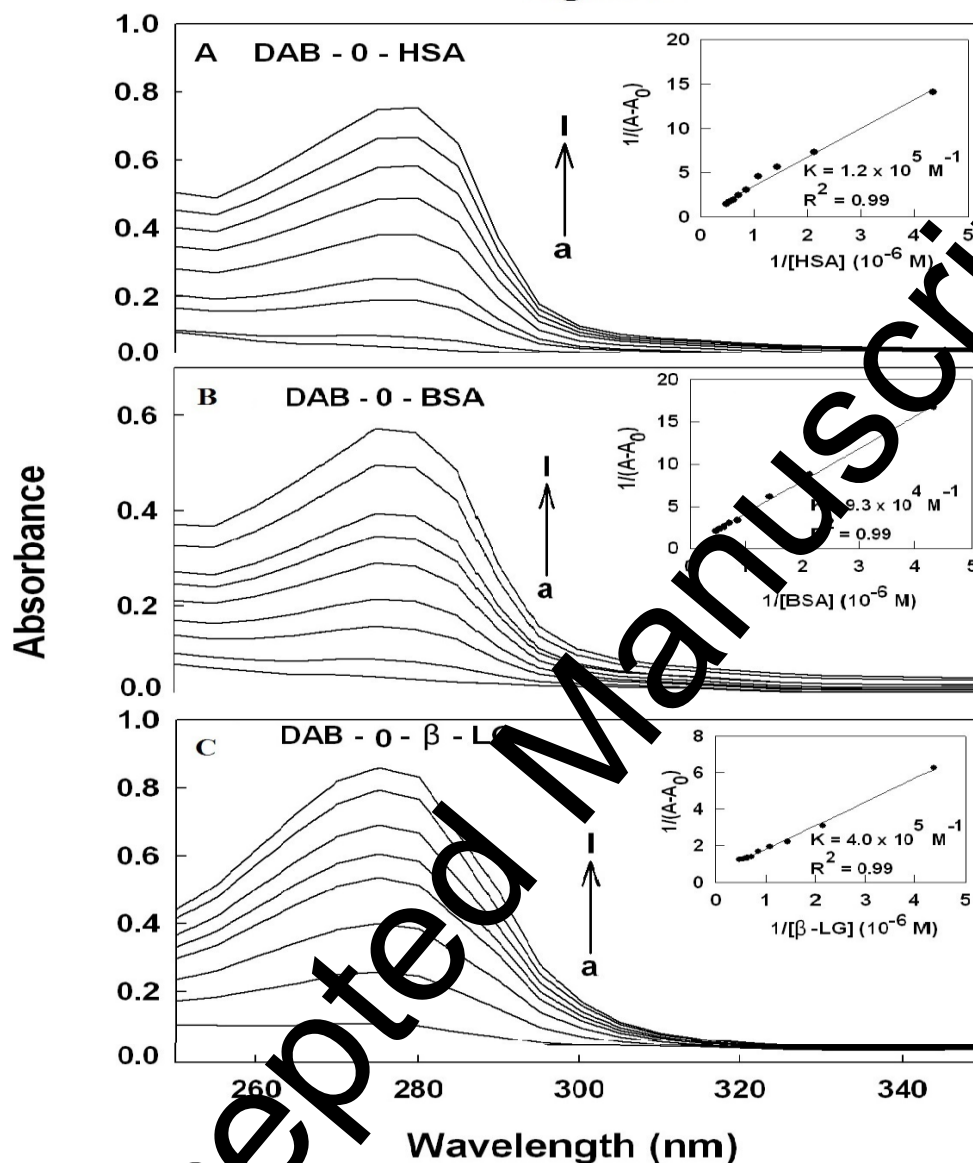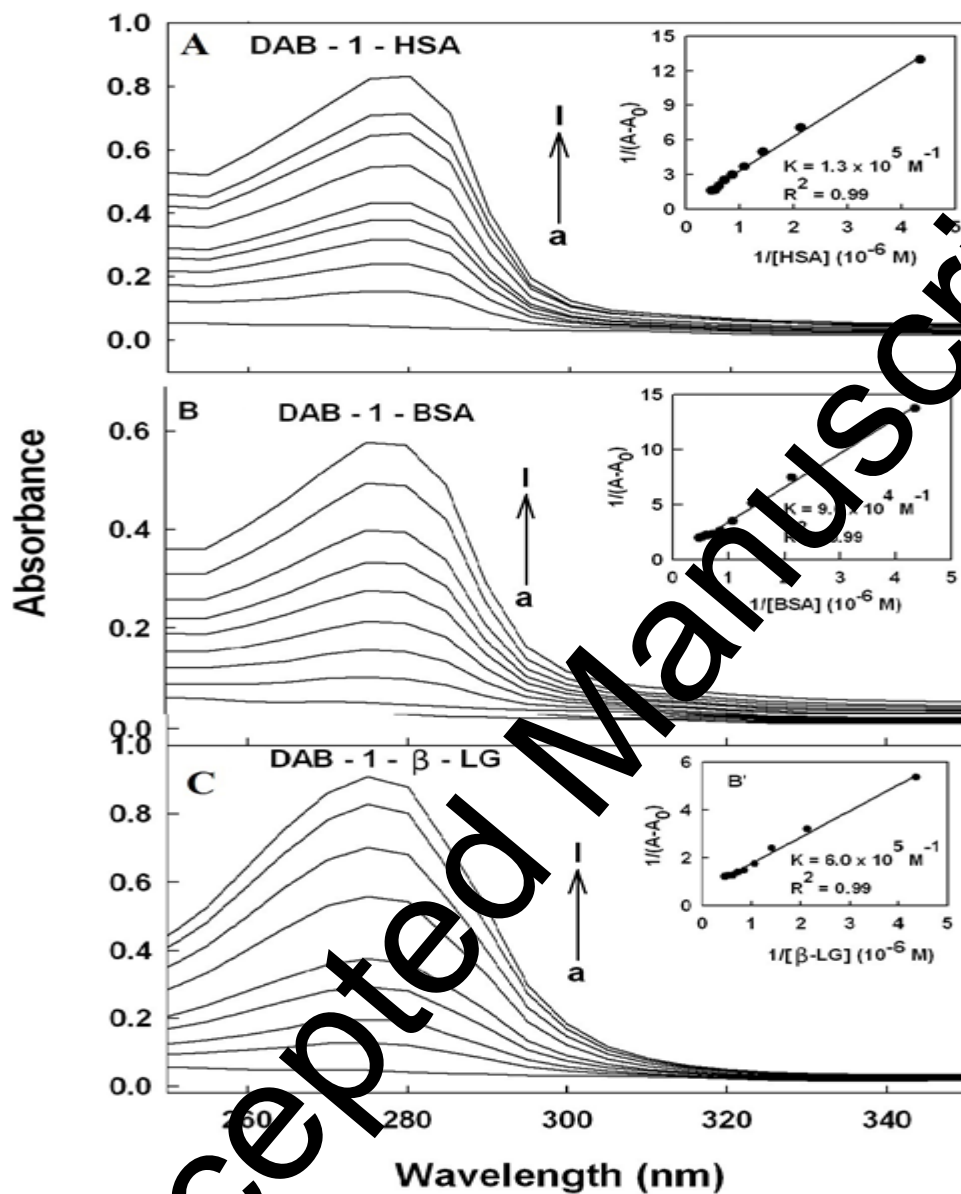
Figure 4

Figure 4. UV-visible spectra of DAB-1 and its conjugates with HSA (A), BSA (B) and β-LG (C) at 60 µM (a) and its DAB-1 complexes (b-i) for DAB-1 at 1, 5, 10, 20, 30, 40, 50 and 60µM; Inset: plot of $1/(A-A_0)$ vs (1/ drug concentration) and binding constants (K) for drug-protein conjugates.

Thermodynamic analysis of DAB-0 and DAB-1-protein adducts

DAB-0 and DAB-1 complexes with serum proteins were further characterized by thermodynamic parameters. Based on the data of ΔH^0 and ΔS^0, the drug-protein interaction can be elucidated (Ross & Subramanian, 1981; Bose, 2016). The thermodynamic parameters for the interaction of drug and protein complexes at 298.15, 308.15 and 318.15 K are presented in **Figs 5, 6** and **Table 2**. The negative sign of ΔG^0 shows that the binding process between drug and protein is spontaneous. Furthermore, all the drug-protein complexes have negative ΔH^0, which means the complex formation between protein and drug is an exothermic reaction. The negative ΔH^0 and positive ΔS^0 for drug-protein conjugates indicate that ionic contacts are observed in the drug-protein complexation (Ross & Subramanian, 1981; Bose, 2016). A detailed thermodynamic analysis of drug-protein interactions shows the importance of the binding constant K, ΔH^0, ΔS^0 and ΔG^0 in determining what type of interaction is predominant in these drug-protein conjugates (Ross & Subramanian, 1981; Bose, 2016; Bekale et al.,, 2015; Bekale et al., 2014). For drug-protein, the enthalpy provides more contribution to ΔG than entropy, which indicates that the binding process is enthalpy driven (**Table 2**).

The binding efficacy for DAB-0 and DAB-1 complexes by serum proteins was determined as reported (Chaudhary et al., 2011). The binding efficacy was estimated to be 40%-50% for drug-HSA, 45-55% for drug-BSA and 45-60% for drug-β-LG systems. The loading efficacy was larger for DAB-1-protein than DAB-0-protein complexes. Hence, a greater amount of DAB-1 can be transported by serum proteins.
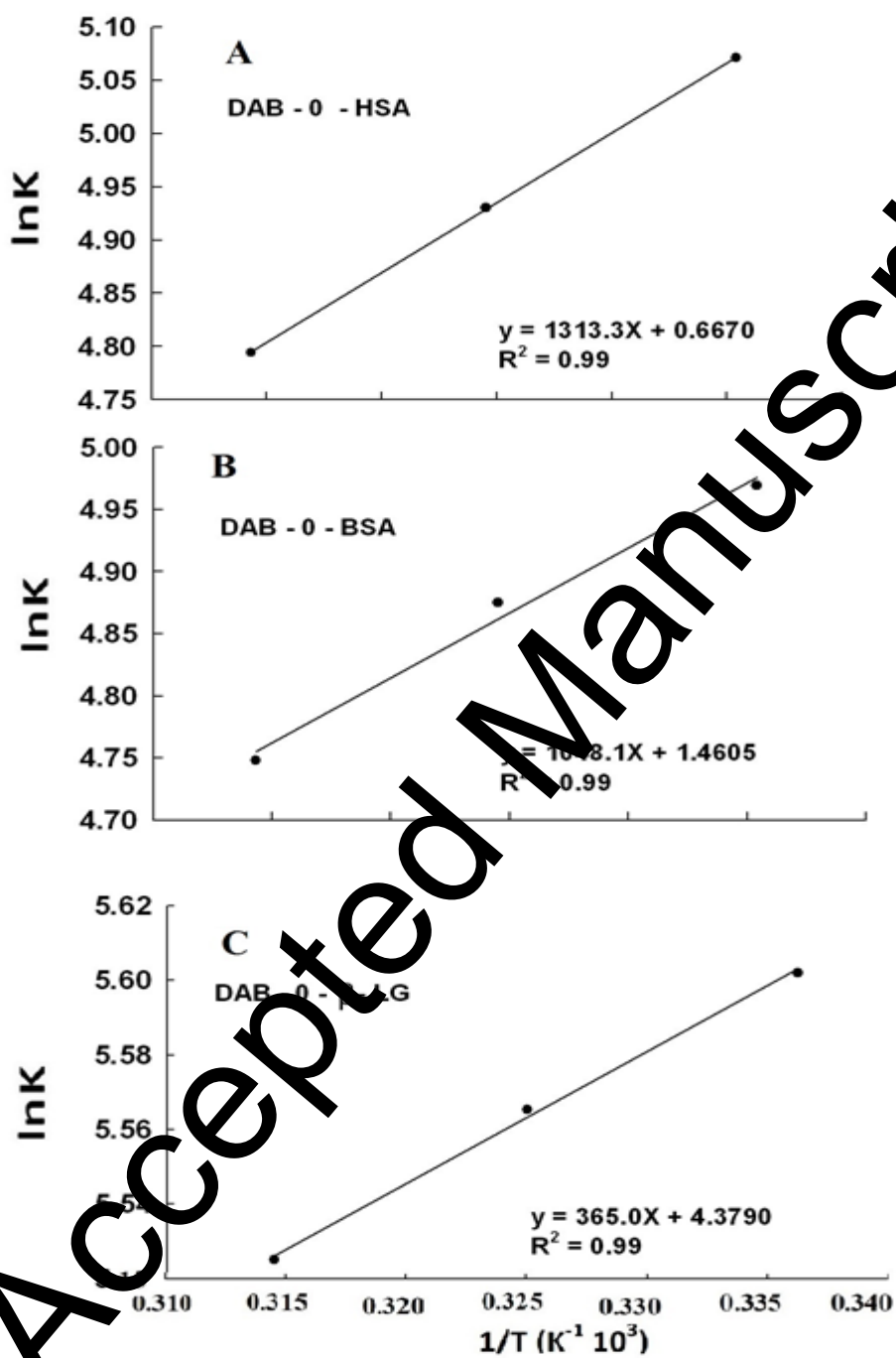
Figure 5

Figure 5. lnK vs 1/T for DAB-0 with HSA (A), BSA (B) and β-LG (C) conjugates.

Figure 6

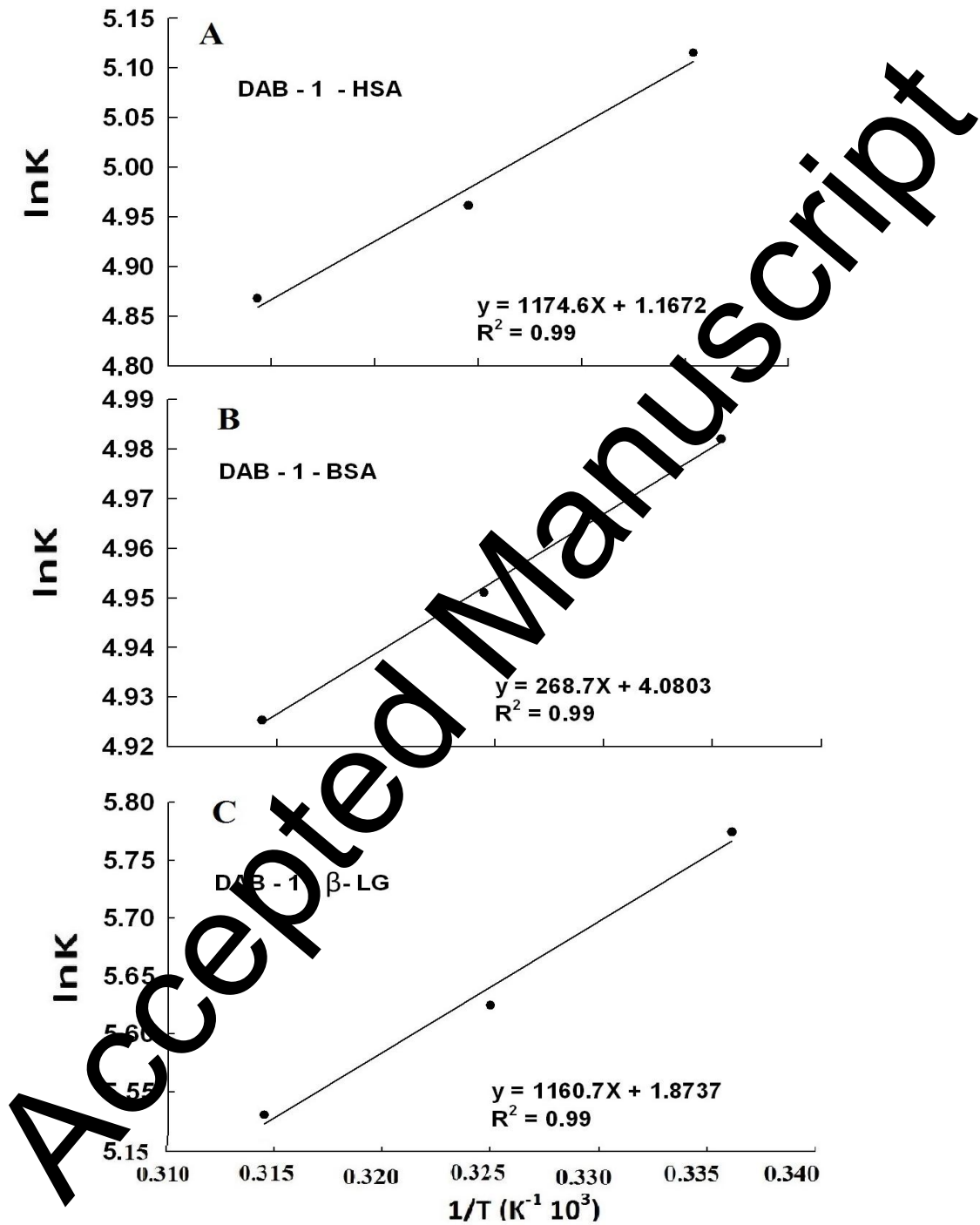**Figure 6**. lnk vs 1/T for DAB-1 with HSA (A), BSA (B) and β-LG (C) conjugates.

Table 2. Thermodynamic parameters for DAB -0 and DAB -1 with serum proteins

Complexes	Thermodynamic parameters			
	ΔH^0 (kJ. mol^{-1})	ΔS^0 (J. mol^{-1}. K^{-1})	$T\Delta S^0$ (kJ. mol^{-1})	ΔG^0 (kJ. mol^{-1})
DAB - 0 – HSA	-10.92	5.55	1.65	-12.57 (298.15 K)
			1.71	-12.63 (308.15 K)
			1.76	-12.68 (318.15 K)
DAB - 1 – HSA	-9.77	9.70	2.89	-12.66 (298.15 K)
			2.99	-12.76 (308.15 K)
			3.09	-12.85 (318.15 K)
DAB - 0 – BSA	-8.71	12.14	3.62	-12.33 (298.15 K)
			3.74	-12.46 (308.15 K)
			3.86	-12.58 (318.15 K)
DAB - 1 – BSA	-2.23	33.92	10.11	-12.35 (298.15 K)
			10.45	-12.69 (308.15 K)
			10.79	-13.03 (318.15 K)
DAB - 0 – β - LG	-3.03	36.41	10.85	-13.89 (298.15 K)
			11.22	-14.25 (308.15 K)

			11.58	-14.62 (318.15 K)
DAB - 1 – β - LG	-9.65	15.58	4.64	-14.29 (298.15 K)
			4.80	-14.45 (308.15 K)
			4.96	-14.61 (318.15 K)

Structural analysis of DAB-0 and DAB-1-protein by FTIR spectroscopy

The conjugation of DAB-0 and DAB-1 with HSA, BSA and *ß*-LG was analyzed by infrared spectroscopy and its derivative methods. Drug-protein interactions alter protein conformation and induce spectral change for protein amide I band at 1659-1657 cm^{-1} (mainly C=O stretch) and amide II band at 1546-1545 cm^{-1} (C-N stretching coupled with N-H bending modes) (Krimm & Bandekar, 1986; Tian et al., 2005; Grdadolnik, 2011). The intensity variations of protein amide I and amide II bands obtained by difference spectra [(protein solution + drug solution) – (protein solution)] are shown in **Figs 7, 8** and **9**.

At low and high drug concentrations (15 to 60 μM), major intensity changes were observed for the protein amide I and amide II, in the difference spectra of the drug-HSA and drug-BSA and drug-β-LG complexes (**Figs 7, 8, 9** and **diffs 15** and **60 μM**). The positive features observed are due to the increase in intensity of amide I and amide II bands located in the difference spectra at 1720-1500 cm^{-1} (**Figs 7, 8, 9** and **diffs 15** and **60 μM**). As drug concentration increased (60 μM), more intensity variations of protein amide I and amide II were observed with stronger features around 1700-1500 cm^{-1} (**Figs 7** and **8, diffs 60 μM**). As drug concentration increased more perturbations of the amide I and amide II were

observed (**diffs 60 μM**). The spectral alterations observed are due to changes in the intensity of the amide I and amide II band, upon drug interactions with protein C-O, C-N and NH groups (hydrophilic contacts) and linked to variations of protein conformation discussed below.

The secondary structures of the free HSA, BSA and β-LG and their drug conjugates are shown in **Table 3**. The free HSA has 57 % α-helix (1656 cm^{-1}), β-sheet 14 % (1628 and 1617 cm^{-1}), turn structure 13 % (1679 cm^{-1}), β-antiparallel 4 % (1689 cm^{-1}) and random coil 12 % (1637 cm^{-1}) (**Table 3**). The free BSA contains α-helix 63% (1656 cm^{-1}), β-sheet 16% (1612 and 1626 cm^{-1}), turn 12% (1678 cm^{-1}), β-antiparallel 3% (1691 cm^{-1}) and random coil 6% (1638 cm^{-1}) (**Table 3**). The free β-LG has major β-sheet 58% (1640, 1623), α-helix 11% (1655 cm^{-1}), turn 14% (1667 cm^{-1}) and β-antiparallel 17% (1679) (**Table 3**). Upon DAB-0 and DAB-1 interactions, a decrease of α-helix from 57% (free HSA) to 37-34% with an increase in random and turn structures (drug-HSA) were observed (**Table 3**). Similarly, for BSA a decrease of α-helix from 63% (free BSA) to 41-38% with an increase of turn and random coil structures (drug-BSA) were observed, upon drug complexation (**Table 3**). However, for β-LG a decrease of β-sheet from 58% (free β-LG) to 46-32% with an increase of α-helix, turn and random structures (drug-β-LG) were observed, upon drug conjugation (**Table 3**).The results showed that major conformational changes occurred for HSA, BSA and β-LG drug complexes, leading to a partial protein destabilization (Essemine et al., 2011; Goñ et al., 2014; Yeggoni et al., 2014). Similar protein conformational changes were observed for HSA, BSA and β-LG upon various ligands complexation (Nerusu et al., 2017; Hasni).

Table 3. Percentage changes in secondary structure contents for serum proteins and their DAB-0 and DAB-1 complexes in hydrated film at pH 7.

Sample	Amide I (cm^{-1}) components				
	α-helix (±2) 1654-1600	β-helix (±1) 1614-1637	random coil (±1) 1638-1648	turn (±2) 1670-1678	β-antiparallel (±1) 1680-1691
Free HSA (250 μm)	57	14	12	13	
DAB - 0 - HSA (250 μm)	37	14	26	14	9
DAB - 1 - HSA (250 μm)	34	13	23	20	10
Free BSA (250 μm)	63	16	6	12	3
DAB - 0 - BSA (250 μm)	41	11	19	16	13
DAB - 1 - BSA (250 μm)	38	10	22	23	7
Free β – LG (250 μm)	11	58	0	14	17
DAB –0-β – LG (250 μm)	32		6	12	4
DAB - 1 - β – LG (250 μm)	67	32	9	13	9

Figure 7

Figure 7. FTIR spectra in the region of 1800-600 cm^{-1} of hydrated films (pH 7.2) for free HSA for with DAB-0 (**A**) and DAB-1 (**B**) (drug 60 µM) and the difference spectra (diff.) of drug-protein conjugates (bottom two curves) obtained at different drug concentrations (indicated on the figure).
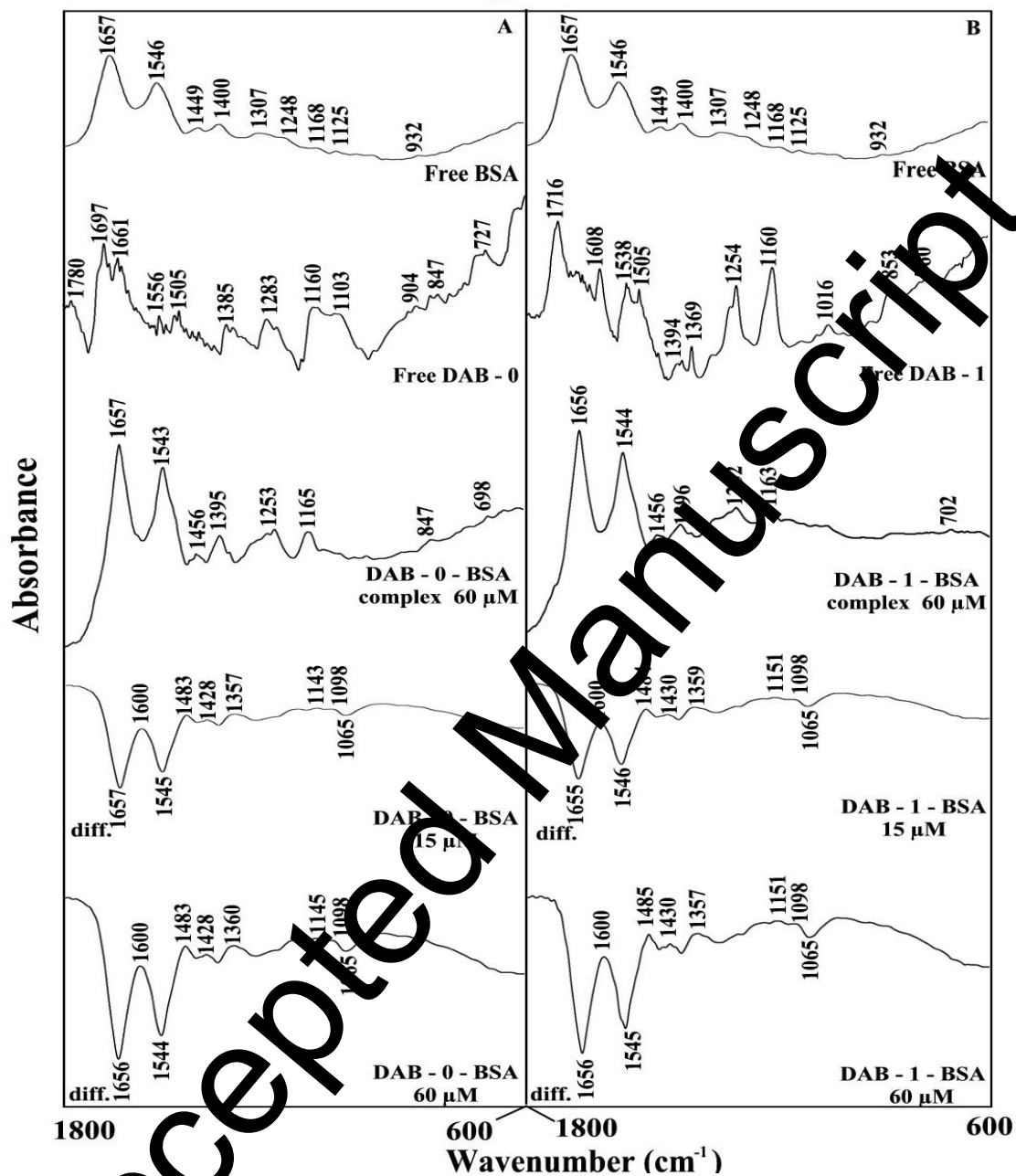
Figure 8

Figure 8. FTIR spectra in the region of 1800-600 cm^{-1} of hydrated films (pH 7.2) for free BSA with DAB-0 (**A**) and DAB-1 (**B**)(drug 60 µM) and the difference spectra (diff.) of drug-protein conjugates (bottom two curves) obtained at different drug concentrations (indicated on the figure).

Figure 9

Figure 9. FTIR spectra in the region of 1800-600 cm^{-1} of hydrated films (pH 7.2) for free β-LG with DAB-0 (A) and DAB-1 (**B**) (drug 60 μM) and the difference spectra (diff.) of drug-protein conjugates (bottom two curves) obtained at different drug concentrations (indicated on the figure).

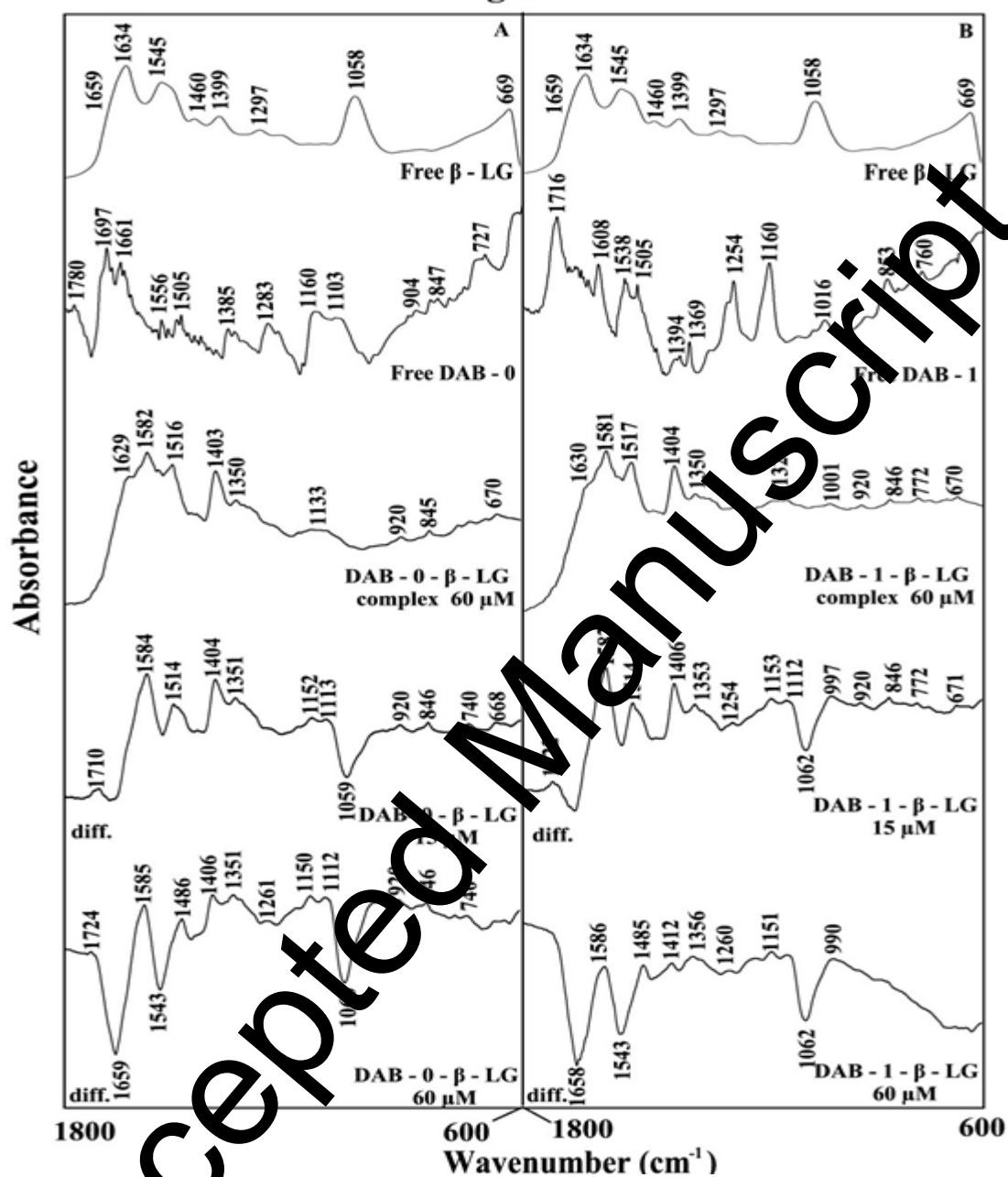*Location of DAB-0 and DAB-1 binding sites on HSA, BSA and b-LG by docking*

Docking results showed that in the DAB-0 and DAB-1 binding HSA *via* different amino acids in drug-HSA adducts, DAB-0 is closed to **Arg-186, Ile-142, Leu-182, Leu-185, Lys-137, Met-123, Phe-134, Phe-165, Tyr-138, Tyr-161** with the free binding energy of -9.7 kcal/mol, while DAB-1 is located in the vicinity of **Ala-210, Glu-479, Leu-481, Lys-199, Phe-206, Phe-211, Ser-202, *Ser-480, Trp-214, *Val-482 (H-bonding)** with binding energy of -9.61 kcal/mol (**Fig. 10A** and **Table 4**). In drug-BSA complexes, DAB-0 binds ***Arg-209 (H-bonding), Asp-142, Cys-147, *Glu-206, Ile-165, Leu-139, Leu-162, Leu-202, Phe-150, Phe-141, Trp158, Tyr-161 with the free energy of** -9.57 kcal/mol, whereas in DAB-1-BSA, drug is surrounded by***Asp-142 (H-bonding), Cys-147, Ile-165, Leu-139, Leu-146, Leu-162, Lys-140, Phe-60, Phe-150, Phe-147, Trp-158, Tyr-161** with the free binding energy of -11.14 kcal/mol (**Fig. 10B and Table 4**). Similarly, in the drug-*β*-LG adducts, DAB-0 is located near **Asn-90, Ile-56, Ile-71, Ile-84, Leu-46, Leu-54, Leu-58, Leu-103, Leu-122, Met-107, Phe-105, Val-41, Val-43, Val-92** with the free binding energy of 11.05 kcal/mol, while DAB-1 binds to **Asn-90, Asp-85, Ile-56, Ile-71, Ile-84, Leu-46, Leu-54, Leu-58, Leu-122, Phe-105, Val-41, Val-43, Val-92** with the free binding energy of -10.77 kcal/mol (**Fig. 10C and Table 4**). As it is shown in **Fig. 10 and Table 4**, DAB-0 and DAB-1 are surrounded by both hydrophilic and hydrophobic amino acids residues. It is worth mentioning that drugs bind to either cysteine or methionine containing sulfur groups (**Table 4**). It is interesting to note that H-bonding systems are established in the drug-HSA and drug-BSA complexes that are not present in drug-*β*-LG adducts (**Fig. 10** and **Table 4**). The free binding energy showed that *β*-LG forms more stable conjugates than HSA and BSA which is in agreement with our experimental results (**Tables 1** and **4**).
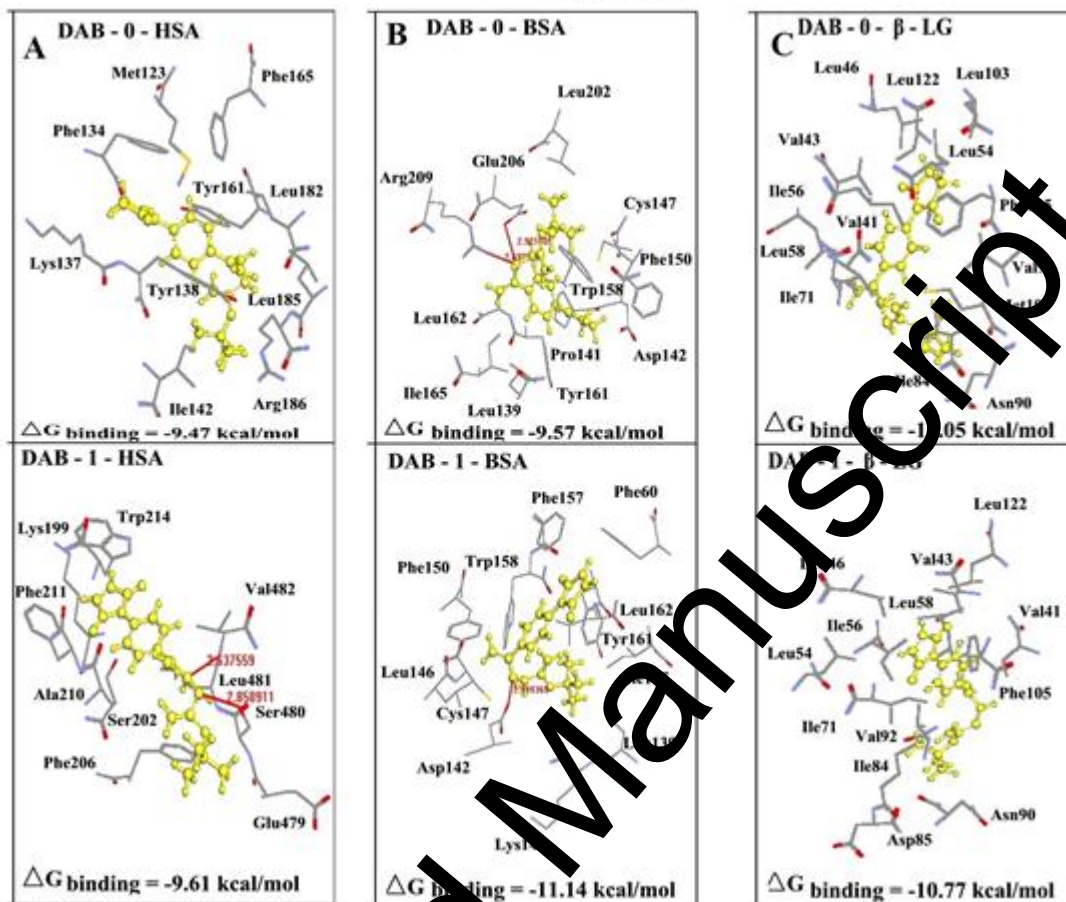
Figure 10

Figure 10. Best docked conformations of drug–HSA (**A**), drug–BSA (**B**) and drug β-LG conjugates (**C**) with the free binding energy.

Table 4. Amino acid residues involved in DAB-0 and DAB-1 with serum proteins interactions and free binding energy for the best selected docking positions.

Complexes	Amino acid residues involved in the interaction	$\Delta G_{binding}$ (kcal/mol)
DAB - 0 – HSA	Arg-186, Ile-142, Leu-182, Leu-185, Lys-137, Met-123, Phe-134, Phe-165, Tyr-138, Tyr-161	- 9.47
DAB - 1 – HSA	Ala-210, Glu-479, Leu-481, Lys-199, Phe-206, Phe-211, Ser-202, *Ser-480, Trp-214, *Val-482	- 9.61
DAB - 0 – BSA	*Arg-209, Asp-142, Cys-147, *Glu-206, Ile-165, Leu-139, Leu-162, Leu-202, Phe-150, Phe-141, Trp158, Tyr-161	- 9.57
DAB - 1 – BSA	*Asp-142, Cys-147, Ile-165, Leu-139, Leu-146, Leu-162, Lys-140, Phe-60, Phe-150, Phe-157, Trp-158, Tyr-161	- 11.14
DAB - 0 – β-LG	Asn-90, Ile-56, Ile-71, Ile-84, Leu-46, Leu-54, Leu-58, Leu-103, Leu-122, Met-107, Phe-105, Val-41, Val-43, Val-92	- 11.05
DAB - 1 – β-LG	Asn-90, Asp-85, Ile-56, Ile-71, Ile-84, Leu-46, Leu-54, Leu-58, Leu-122, Phe-105, Val-41, Val-43, Val-92	- 10.77

Concluding remarks

The distinct biological properties shown by DAB-0 and DAB-1 (anti-proliferative, anti-inflammatory and regulation of cell signaling pathways) prompt us to investigate the interaction of these molecules with transport proteins. It is well known that serum proteins are widely used in clinical settings as a drug delivery system due to their potential for improving targeting while decreasing the side effects of drugs. DAB-0 and DAB-1 bind serum proteins via ionic contacts with β-LG forming more stable conjugates than HSA and

BSA. DAB-1 forms stronger protein adducts than DAB-0, which could at least partly explain the overall inactivity of the latter drug. The binding efficacies were 40% to 50% for DAB-0 and 45% to 60% for DAB-1-protein adducts. Drug complexation induced major perturbations of protein conformations leading to structural destabilization. Serum proteins can be used for the delivery of DAB-1 *in vitro*.

References

Ahmed Ouameur, A., Diamantoglou, S., Sedaghat-Herati, M. R., Nafisi, Sh., Carpentier, R., & Tajmir-Riahi, H. A. (2006). An overview of drug binding to human serum albumin: Protein folding and unfolding. *Cell Biochem. Biophys. 45*, 203

Akdogan, Y., Reichenwallner, J., & Hinderberger, D. (2012). Evidence for water-tuned structural differences in proteins: An approach emphasizing variations in local hydrophilicity. *PLoS ONE 7*, 1–11, e456810.

Arnold, K., Bordoli, A.K., Kopp, L., & Schwede, T. (2006). A web-based environment for protein structure homology modeling. *Bioinformatics 22*, 195–201.

Beauchemin, R., N'soukpoe-Kossi, C.N., Thomas, T.J., Thomas, T., Carpentier, R., & Tajmir-Riahi, H. A. (2007). Polyamine analogues bind human serum albumin. *Biomacromolecules 8*, 3177–3183. 2017/177316 A1.

Belgorosky, D., Langle, Y., Prack Mc Cormick, B., Colombo, L., Sandes, E., & Eiján, A.M. (2014). Inhibition of nitric oxide is a good therapeutic target for bladder tumors that express iNOS. *Nitric Oxide 36*, 11-18.

Bekale, L., Agudelo, D., & Tajmir-Riahi, H.A. (2015). Effect of polymer molecular weight on chitosan-protein interaction. *Colloids Surf. B 125*, 309–317.

Bekale, L., Chanphai, P., Sanyakamdhorn, S., Agudelo, D., & Tajmir-Riahi, H. A. (2014). Microscopic and thermodynamic analysis of PEG-lactoglobulin interaction. *RSC Adv. 4,* 31084–31093.

Belgorosky, D., Langle, Y., Prack Mc Cormick, B., Colombo, L., Sandes, E., & Eiján, A.M. (2014). Inhibition of nitric oxide is a good therapeutic target for bladder tumors that express iNOS. *Nitric Oxide 36*, 11-18.

Bérubé, G., & Reyes-Moreno, C. (2017). Aminobenzoic acid derivatives for use as anti-inflammatory agents, antimetastatic agents and/or anticancer agents. WO2017/177316 A1.

Bose, A. (2016). Interaction of tea polyphenols with serum albumins: A fluorescence spectroscopic analysis. *J. Lumin. 169,* 220–226.

Bourassa, P., Hasni, I., & Tajmir-Riahi, H. A. (2011). Folic acid complexes with human and bovine serum albumins. *Food Chem. 129*, 1148–1155.

Byler, D.M., & Susi, H. (1986). Examination of the secondary structure of proteins by deconvoluted FTIR spectra. *Biopolymers 25*, 469–487.

Carmichael, J., DeGraff, W.G., Gazdar, A.F., Minna, J.D., & Mitchell, J.B. (1987).

Evaluation of a tetrazolium-based semiautomated colorimetric assay: assessment

of chemosensitivity testing. *Cancer Res. 47*, 936-942.

Chandra, S., Dietrich, S., Lang, H., & Bahadur, D. (2011). Dendrimer–doxorubicin

conjugate for enhanced therapeutic effects for cancer. *J. Mater. Chem. 21*, 5729–

5737.

Chanphai, P., Vesper, A. R., Bekale, L., Bérubé, G., & Tajmir-Riahi, H. A. (2015).

Encapsulation of testosterone and its aliphatic and aromatic dimers by milk beta-

lactoglobulin. *Int. J. Biol. Macromol. 76,* 153–160.

Chanphai, P., Vesper, A. R., Bekale, L., Bérubé, G., & Tajmir-Riahi, H. A. (2015).

Transporting testosterone and its dimers by serum proteins. *J. Photochem. Photobiol. B.*
153, 173–183.

Chanphai, P., Ouellette,V., Bérubé, G., & Tajmir-Riahi, H. A. (2018). Conjugation of testo

and testo-Pt(II) with serum proteins: Loading efficacy and protein conformation. *Int. J. Biol.*

Macromol. 118, 1112–1119.

Collini, M., D'Alfonso, L., & Baldini, G. (2000). New insights on β-lactoglobulin binding

sites by 1-anilinonaphthalene-8-sulfonate fluorescence decay. Protein Sci. 9, 1968-1974.

Colotta, F., Allavena, P., Sica, A., Garlanda, C., & A. Mantovani, A. (2009). Cancer-related

inflammation, the seventh hallmark of cancer: links to genetic instability. *Carcinogenesis,*

30, 1073-1081.

Dai, X., Yan, J., Fu, X., Pan, Q., Sun, D., Xu, Y., Wang, J., Nie, L., Tong, L., Shen, A.,

Zheng, M., Huang, M., Tan, M., Liu, H., Huang, X., Ding, J., & Geng, M. (2017). Aspirin

inhibits cancer metastasis and angiogenesis via targeting heparanase. *Clin. Cancer Res. 23,* 6267-6278.

Dallagi, A., Girouard, J., Hamelin-Morrissette, J., Dadzie, R., Laurent, L., Vaillancourt, C., Lafond, J., Carrier, C., & Reyes-Moreno, C. (2015). The activating effect of IFN-gamma on monocytes/macrophages is regulated by the LIF-trophoblast-IL-10 axis via Stat1 inhibition and Stat3 activation. *Cell Mol. Immunol. 12,* 326-341.

Dousseau, F., Therrien, M., & Pezolet, M., (1989). On the spectral subtraction of water from the FT-IR spectra of aqueous solutions of proteins. *Appl. Spectrosc. 43,* 538–542.

Dufresne, M., Dumas, G., Asselin, E., Carrier, C., Pouliot, M., & Reyes-Moreno, C. (2011). Pro-inflammatory type-1 and anti-inflammatory type-2 macrophages differentially modulate cell survival and invasion of human bladder carcinoma T24 cells. *Mol Immunol. 48,* 1556-1567.

Dumas, G., Dufresne, M., Asselin, E., Girouard, J., Carrier, C., & Reyes-Moreno, C. (2013). CD40 pathway activation reveals dual function for macrophages in human endometrial cancer cell survival and invasion. *Cancer Immunol. Immunother. 62,* 273-283.

Elsadek, B., & Kratz, F. (2012). Impact of albumin on drug-delivery-new application on the horizon. J. *Control. Release 157*, 4-28.

Essemine, J., Hasni, I., Caprpentier, R., Thomas, T. J., & Tajmir-Riahi, H.A. (2011).Binding of biogenic and synthetic polyamines to *β*-lactoglobulin. *Int. J. Biol. Macromol. 49*, 201-211.

Fabris, V.T., Lodillinsky, C., Pampena, M.B., Belgorosky, D., Lanari, C., & Eiján, A.M. (2012). Cytogenetic characterization of the murine bladder cancer model MB49 and the derived invasive line MB49-I. *Cancer Genet. 205,* 168-176.

Ghuman, J., Zunszain, P.A., Petitpas, I., A.A. Bhattacharya, A. A., Otagiri, M., & Curry, S. (2005). Structural basis of the drug-binding specificity of human serum albumin. *J. Mol. Biol. 353*, 38-52.

Gokara, M., Kimavath, G.B., Podile, A.R., & Subramanyam. R. (2014). Differential interactions and structural stability of chitosan oligomers with human serum albumin and α-1-glycoprotein. *J. Biomol. Struct. Dyn. 33*,196–210.

Grdadolnik, J. (2003). Saturation effects in FTIR spectroscopy: intensity of amide I and amide II bands in protein spectra. *Acta Chim. Slov. 50*, 777-788.

Hamelin-Morrissette, J., Cloutier, S., Girouard, J., Belgorosky, D., Eijan, A.-M., Legault, J., Bérubé, G., & Reyes-Moreno. C. (2015). Identification of an anti-Inflammatory derivative with anti-cancer potential: The impact of each of its structural components on inflammatory responses in macrophages and bladder cancer cells. *Eur. J. Med. Chem. 96*, 259-268.

Hasni, I., Bourassa, P., & Tajmir-Riahi, H. A. (2011). Binding of cationic lipids to milk *β*-lactoglobulin. *J. Phys. Chem. B 115*, 6683-6690.

Jameson, G.B., Adams, J.J., & Creamer, L.K. (2002). Flexibility, functionality and hydrophobicity of bovine *β*-lactoglobulin. *Int. Dairy J. 12*, 319–329.

Krasowil, N. A., Huber, W., Müller, F., Kansy, M., & Gerber, P.R. (2002). Predicting plasma protein binding of drugs: a new approach. *Biochem. Pharmacol. 64* 1355-1374.

Kratz, F., Elsadek, B. (2012). Clinical impact of serum proteins on drug delivery. *J. Control. Release 161*, 429–445

Kratz, F. (2008). Albumin as a drug carrier: Design of prodrugs, drug conjugates and nanoparticles. *J. Control. Release 132*, 171–183.

Krimm, S., & Bandekar, J. (1986).Vibrational spectroscopy and conformation of peptides, polypeptides, and proteins. *Adv. Protein. Chem. 38*, 181–364.

Leduc, K., Bourassa,V., Asselin, E., Leclerc, P., Lafond, J., & Reyes-Moreno, C. (2012). Leukemia Inhibitory Factor Regulates Differentiation of Trophoblast-Like BeWo Cells Through the Activation of JAK/STAT and MAPK3/1 MAP Kinase-Signaling Pathways. *Biol. Reprod. 86*, 1-10.

Loch, J. J., Bonarek,P., Polit, A., Swiatek, S., Czuba,M., Ludwikowska, M., & Lewinski, K. (2015). Conformational variability of goat beta-lactoglobulin: crystallographic and thermodynamic studies. *Int. J. Biol. Macromol.* 72, 1283–1291.

Nakamura, K., & Smyth, M.J. (2017). Targeting cancer-related inflammation in the era of immunotherapy. Immunology and cell biology. 95, 325-332.

Nerusu, A., Reddy, P.S., Ramachary, D.B., & Subramanyam, R. (2017). Unraveling the stability of plasma proteins upon interaction of synthesized androstenedione and its derivatives—A biophysical and computational approach. *ACS Omega 2*, 6514–6524.

Painter, L., Harding, M.M., & Beeby, P.J. (1998). Synthesis and interaction with human serum albumin of the first 3,18-disub-stituted derivative of bilirubin, *J. Chem. Soc. Perkin Trans 18*, 3041-3044.

Ross, P.D., & Subramanian, S. (1981). Thermodynamics of protein association reactions: forces contributing to stability. *Biochemistry 20*, 3096–3102.

Rost, B. (1999). Twilight zone of protein sequence alignment. *Protein Eng. 12,* 85–94.

Sugio, S., Kashima, A., Mochizuki, S., Noda, M., & Kobayashi, K. (1999). Crystal structure of human serum albumin at 2.5 A ° resolution. *Protein Eng. 12*, 439–44.

Sui, X., Lei, L., Chen, L., Xie, T., & Li, X. (2017). Inflammatory microenvironment in the initiation and progression of bladder cancer. *Oncotarget. 8,* 93279-93294.

Tian, J., Liu, J., Hu, Z., & Chen, X. (2005). Binding of the scutellarin to albumin using tryptophan fluorescence quenching, CD and FT-IR spectra. *Am. J. Immunol. 1,* 21–23.

Yang, F., Zhang, Y., & Liang, H. (2014). Interactive association of drugs binding to human serum albumin. *Int. J. Mol. Sci. 15,* 3580-3595.

Yeggoni, D.P., Gokara, M., Manidhar, D.M., Rachamallu, A., Nakka, S., Reddy, C.S., & Subramanyam, R. (2014). Binding and molecular dynamics studies of 7-hydroxycoumarin derivatives with human serum albumin and their pharmcological importance. *Mol. Pharm. 11*, 1117–1131.

Zhong, W., Wang, Y., Yu, J.S., Liang, Y., Ni, K., & Tu, S. (2004). The interaction of human serum albumin with a novel antidiabetic agent-SU-118. J. Pharm. Sci. 93, 1039–1046.

Zhu, Z., Shen, Z., & Xu, C. (2012). Inflammatory pathways as promising targets to increase chemotherapy response in bladder cancer. *Mediators inflamm.* 52869.